Supplemental Information

Reducing Irradiation Damage In A Long-Life Fast Reactor With Spectral Softening

AG Osborne, MR Deinert

Department of Mechanical Engineering, The Colorado School of Mines

Supplementary Note 1. Monte Carlo Uncertainties. Burnup simulations done in Serpent 2.1.28 tracked 19.2 million neutron histories per burnup step, using 12,000 neutron source points with 800 inactive and 800 active k_{eff} cycles. The Monte Carlo uncertainties are shown as error bars, and do not take into account the uncertainties in the underlying nuclear constants. Error bars are extremely small due to the large number of neutron tracks tallied.

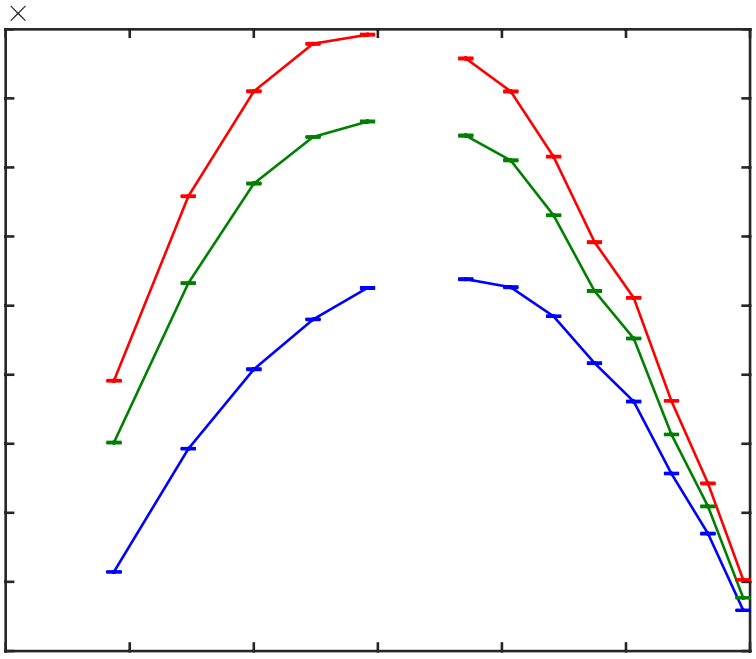

Figure S1. Neutron flux profiles. Results are for the softened metal oxide (MOX) core. Curves at the beginning, middle, and end of life are shown for the core axial centerline, corresponding to the axial position, $180 \leq z \leq 220$ cm. Discontinuities are due to sodium-diluent regions.

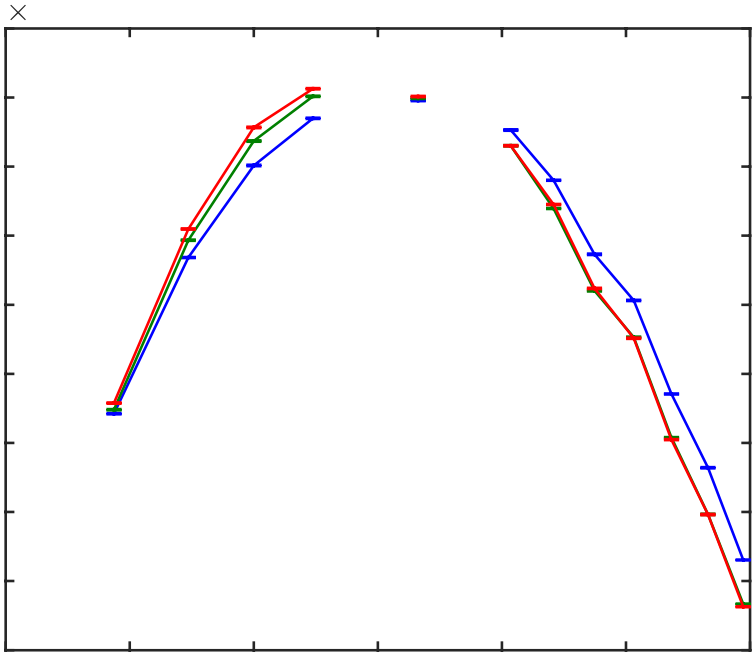

Figure S2. Neutron flux profiles. Results are for the softened MOX core. Curves at the beginning, middle, and end of life are shown for the axial positions, $80 \leq z \leq 100$ cm and $300 \leq z \leq 320$ cm, due to axial symmetry. Discontinuities are due to sodium-diluent regions.

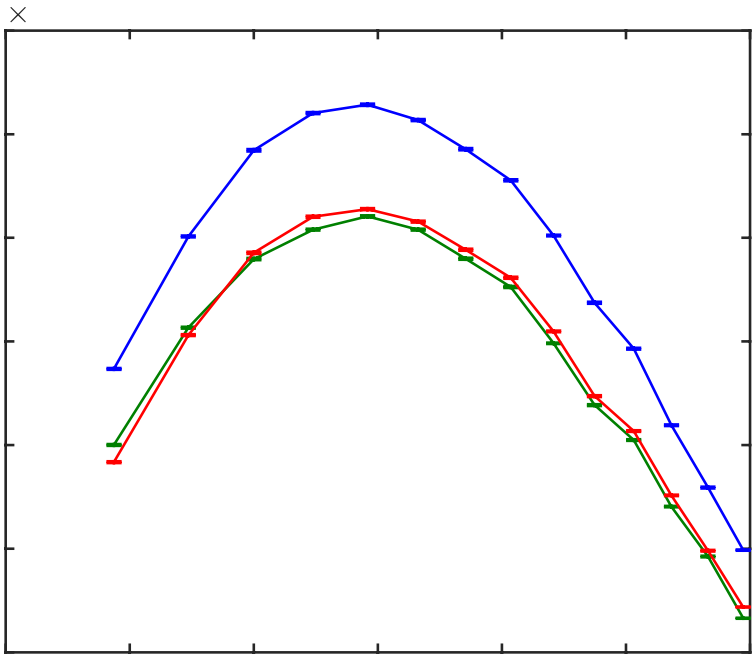

Figure S3. Neutron flux profiles. Results are for the softened MOX core. Curves at the beginning, middle, and end of life are shown for the bottom and top of the core, corresponding to the axial positions, $0 \leq z \leq 20$ cm and $380 \leq z \leq 400$ cm, due to axial symmetry.

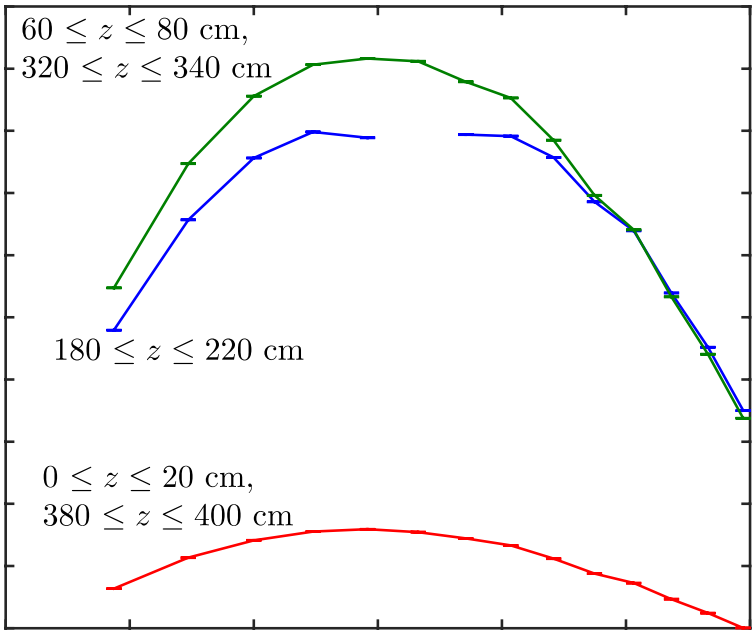

Figure S4. DPA profiles. Results are for the softened MOX core. Curves at the end of life are shown for the core axial centerline (180 ≤ z ≤ 220 cm), bottom and top (0 ≤ z ≤ 20 cm and 380 ≤ z ≤ 400 cm, respectively), and the axial positions that experienced the greatest damage (60 ≤ z ≤ 80 cm and 320 ≤ z ≤ 340 cm). Discontinuities are due to sodium-diluent regions.

Supplementary Note 2. Effect of Beryllium on Power and Neutron Multiplication Factor.

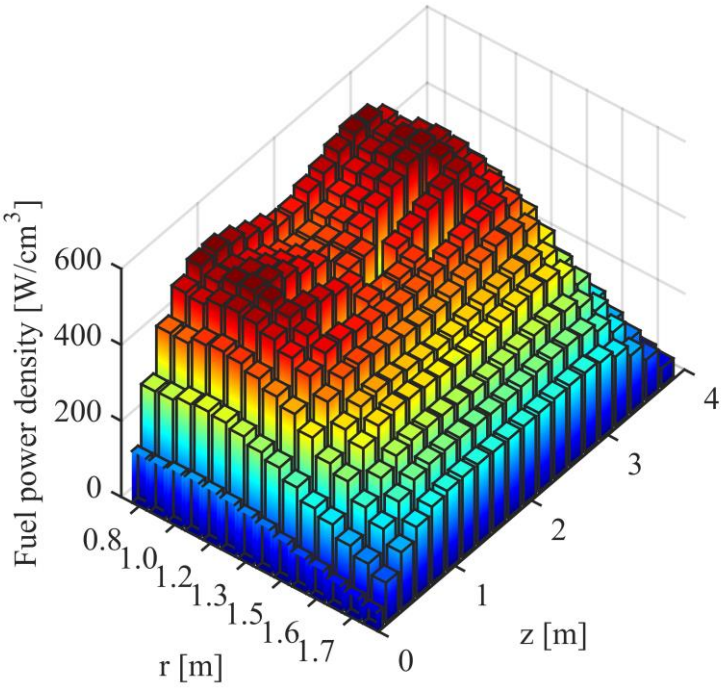

Figure S5. Power density profile for the unsoftened metal core. The profile was evaluated at the beginning of life of the core.

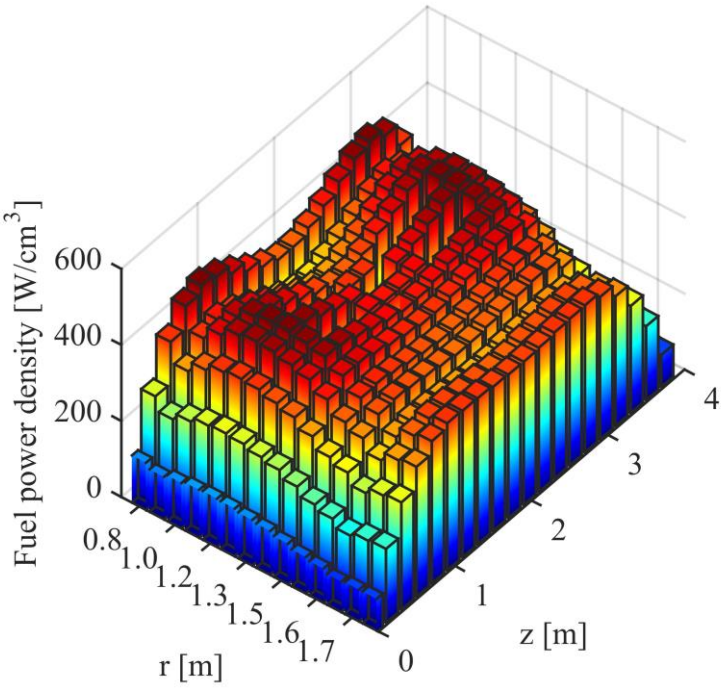

Figure S6. Power density profile for the softened metal core. The profile was evaluated at the beginning of life of the core. An increase in power density is clearly visible at the inner and outer regions, close to the beryllium reflectors.

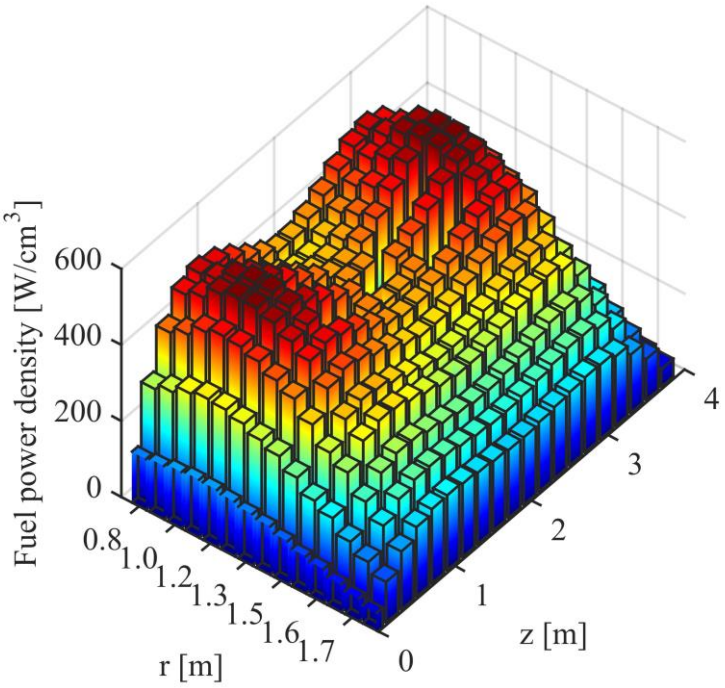

Figure S7. Power density profile for the unsoftened MOX core. The profile was evaluated at the beginning of life of the core.

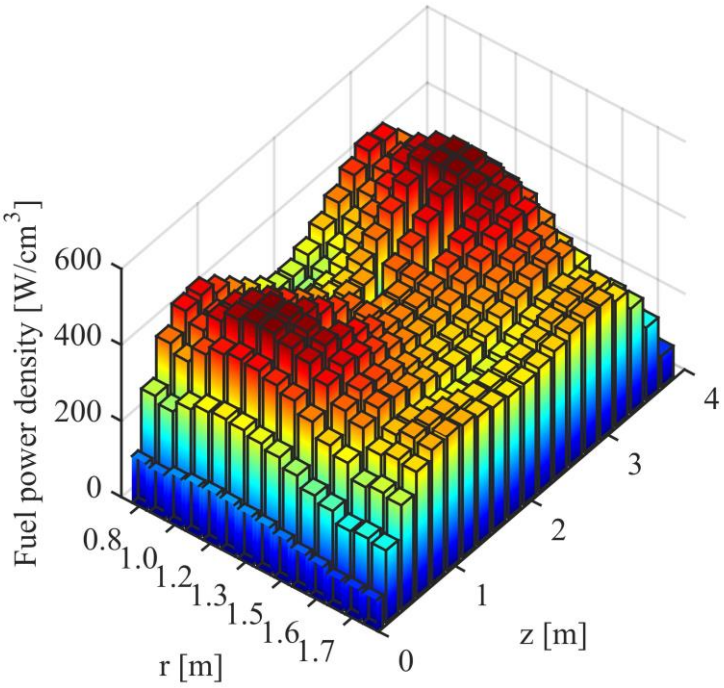

Figure S8. Power density profile for the softened MOX core. The profile was evaluated at the beginning of life of the core. An increase in power density is clearly visible at the inner and outer regions, close to the beryllium reflectors.

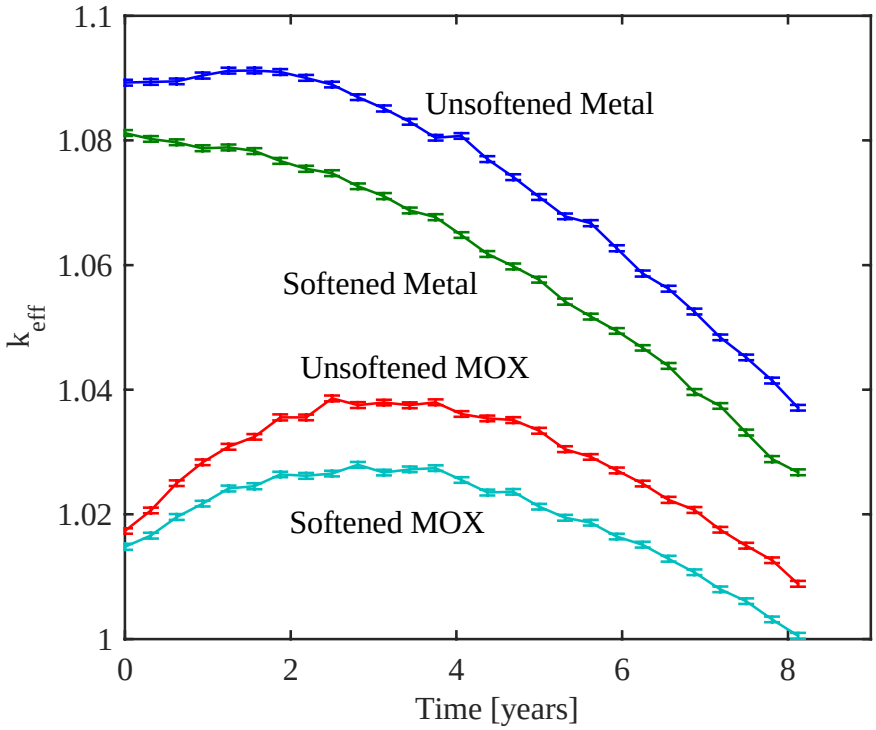

Figure S9. Neutron Multiplication Factor. The curves of the criticality eigenvalue (keff) show that reactivity dropped significantly as the concentration of light elements (oxygen and beryllium) increased.

Supplementary Note 3. Assembly Level Core Geometry and Materials. In order to evaluate the effect of spectral softening on an even basis, all four core designs had the same assembly layout, consisting of an inner reflector region surrounded by annular diluent regions, and an outer reflector. The four cores had the same actinide profiles, which were graded as shown in Figures S10–S19.

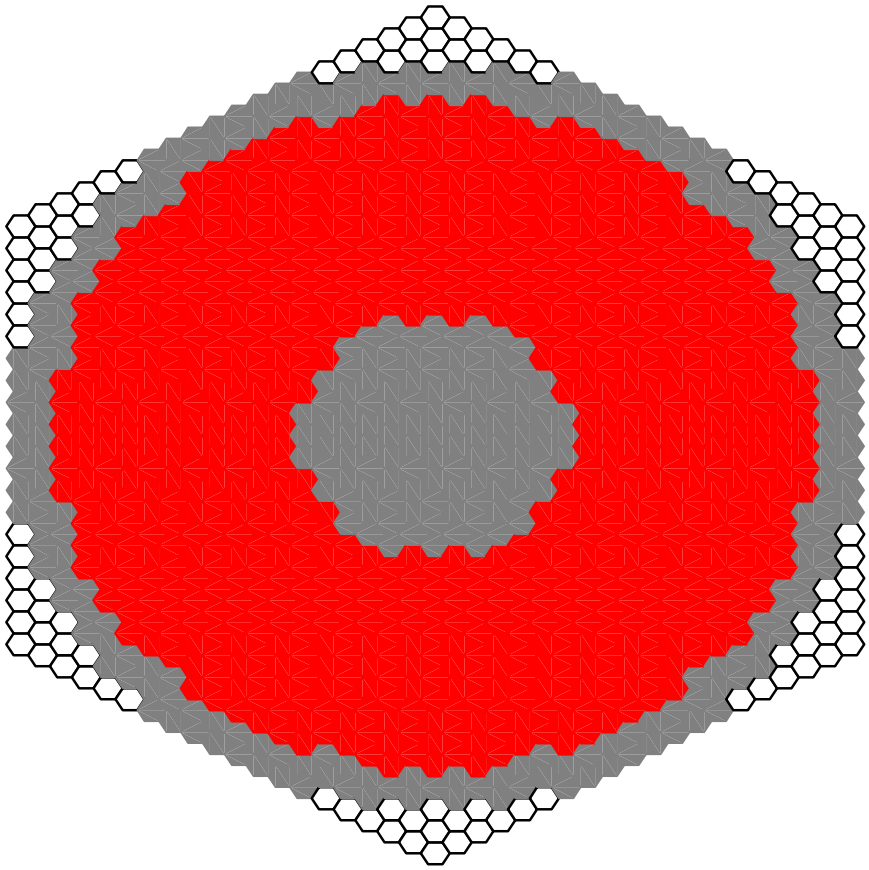

Figure S10. Core geometry and plutonium grading at axial locations z = 0–20 cm and 380–400 cm. Reflector assemblies are in gray, and fuel assemblies contained a uniform plutonium concentration of 16 atom percent of heavy metal. Assembly locations in white were filled with coolant.

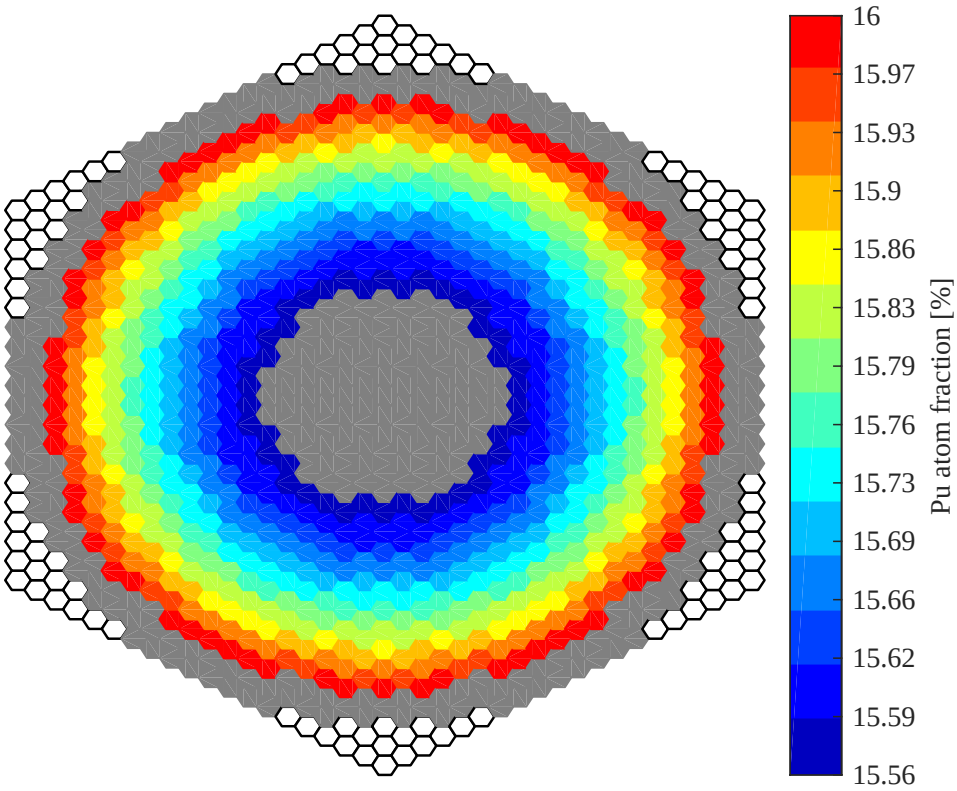

Figure S11. Core geometry and plutonium grading at axial locations z = 20–40 cm and 360–380 cm. Reflector assemblies are in gray, and fuel assemblies contained a graded plutonium concentration of 15.56 to 16 atom percent of heavy metal. Assembly locations in white were filled with coolant.

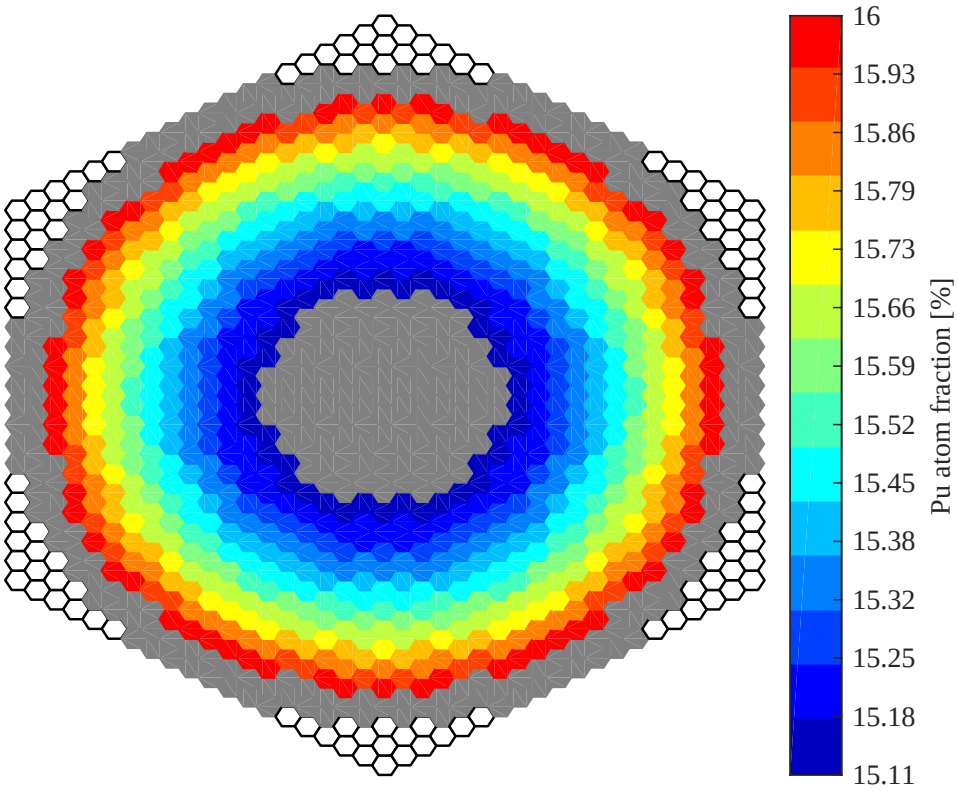

Figure S12. Core geometry and plutonium grading at axial locations z = 40–60 cm and 340–360 cm. Reflector assemblies are in gray, and fuel assemblies contained a graded plutonium concentration of 15.11 to 16 atom percent of heavy metal. Assembly locations in white were filled with coolant.

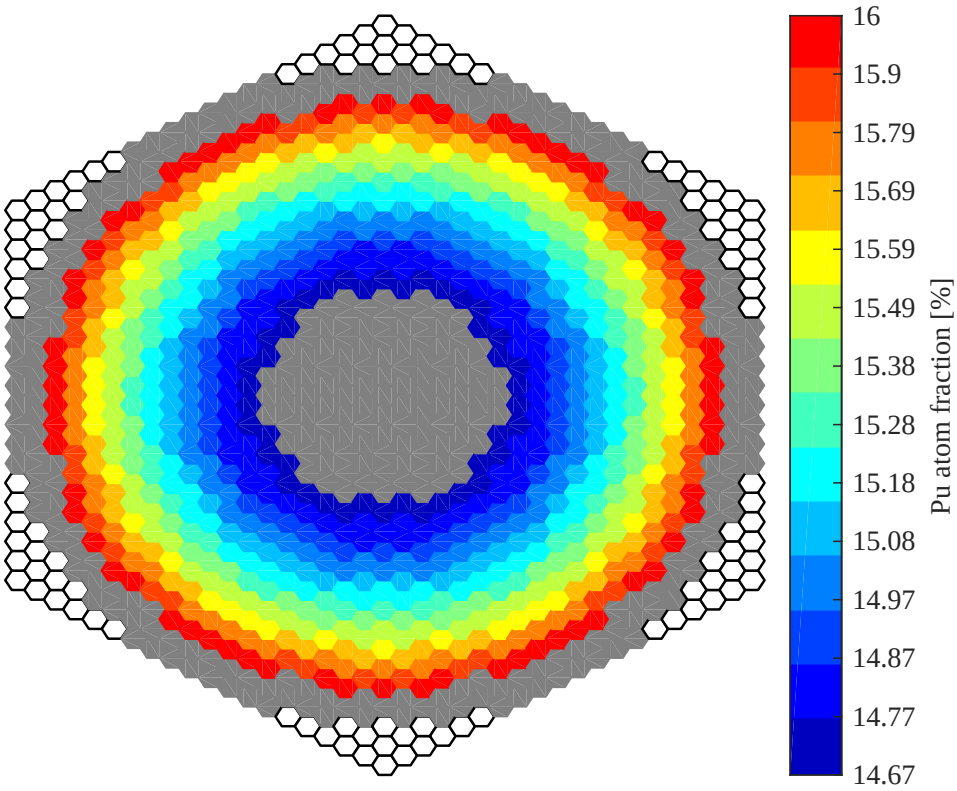

Figure S13. Core geometry and plutonium grading at axial locations z = 60–80 cm and 320–340 cm. Reflector assemblies are in gray, and fuel assemblies contained a graded plutonium concentration of 14.67 to 16 atom percent of heavy metal. Assembly locations in white were filled with coolant.

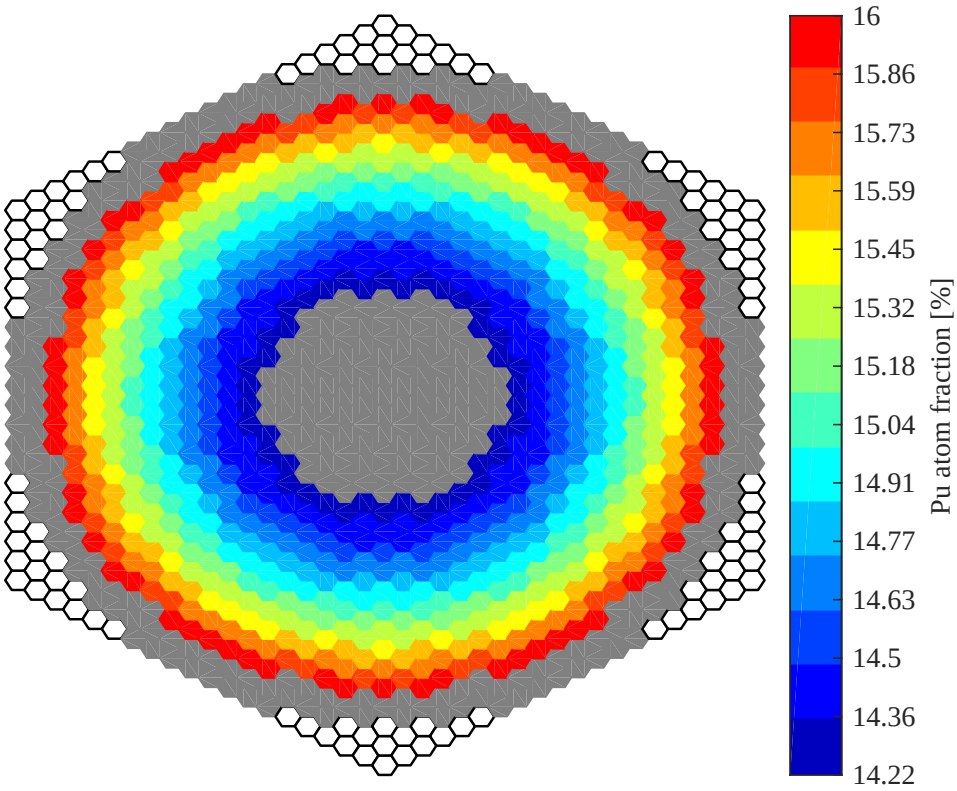

Figure S14. Core geometry and plutonium grading at axial locations z = 80–100 cm and 300–320 cm. Reflector assemblies are in gray, and fuel assemblies contained a graded plutonium concentration of 14.22 to 16 atom percent of heavy metal. Assembly locations in white were filled with coolant.

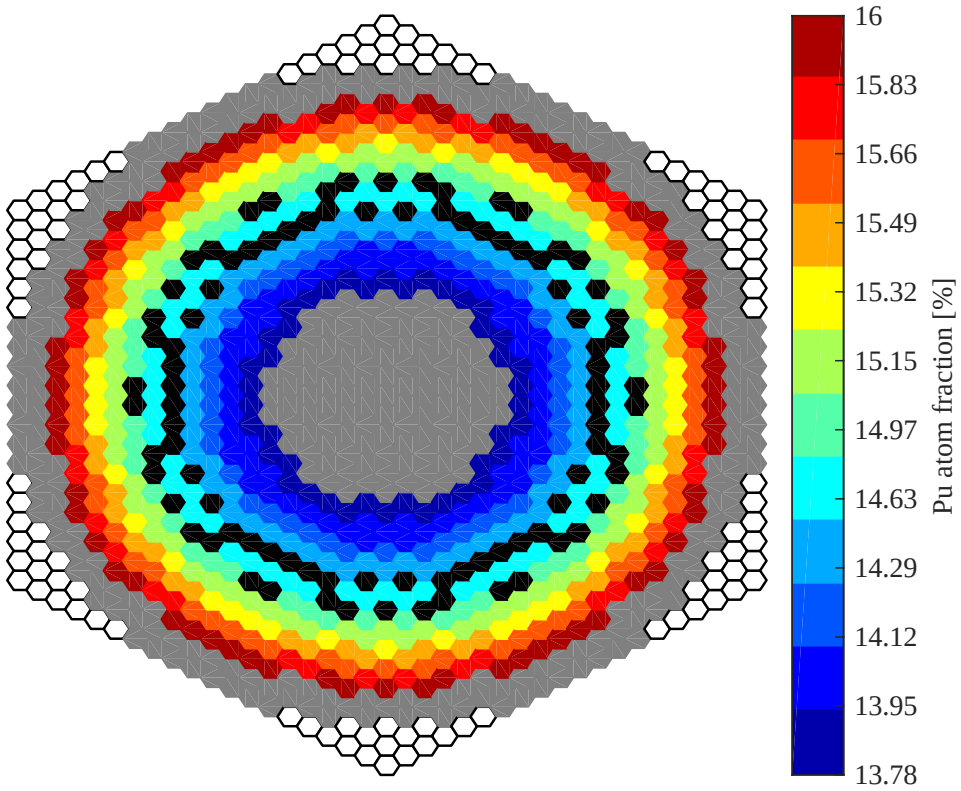

Figure S15. Core geometry and plutonium grading at axial locations z = 100–120 cm and 280–300 cm. Reflector assemblies are in gray, and fuel assemblies contained a graded plutonium concentration of 13.78 to 16 atom percent of heavy metal. Diluent assemblies are shown in black. Assembly locations in white were filled with coolant.

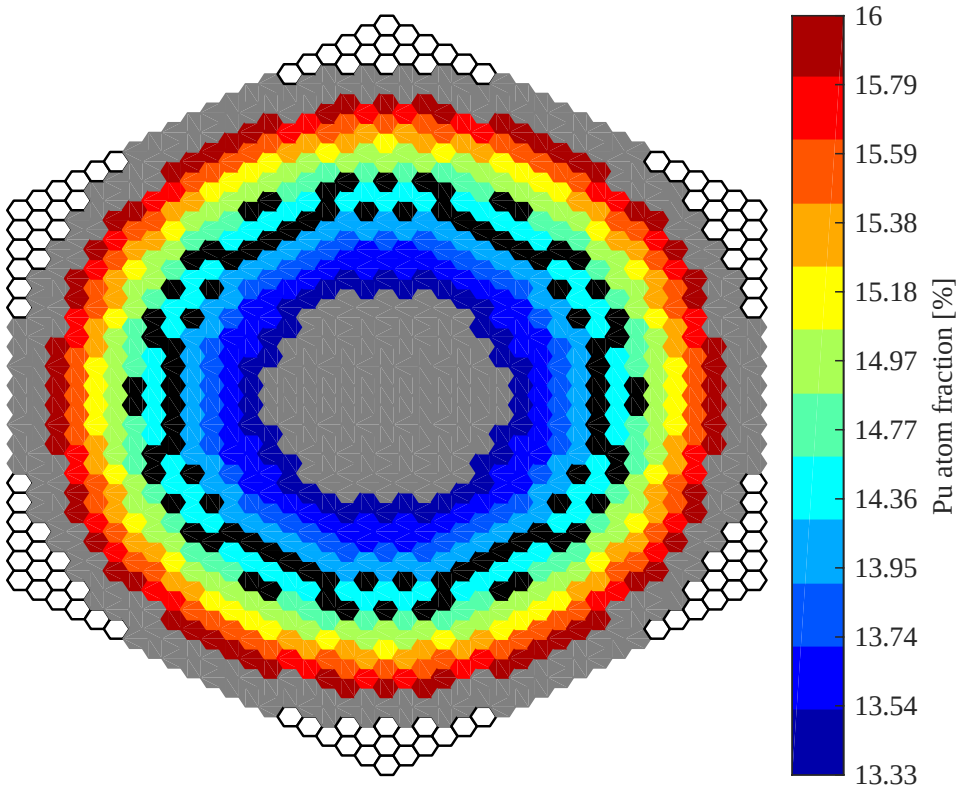

Figure S16. Core geometry and plutonium grading at axial locations z = 120–140 cm and 260–280 cm. Reflector assemblies are in gray, and fuel assemblies contained a graded plutonium concentration of 13.33 to 16 atom percent of heavy metal. Diluent assemblies are shown in black. Assembly locations in white were filled with coolant.

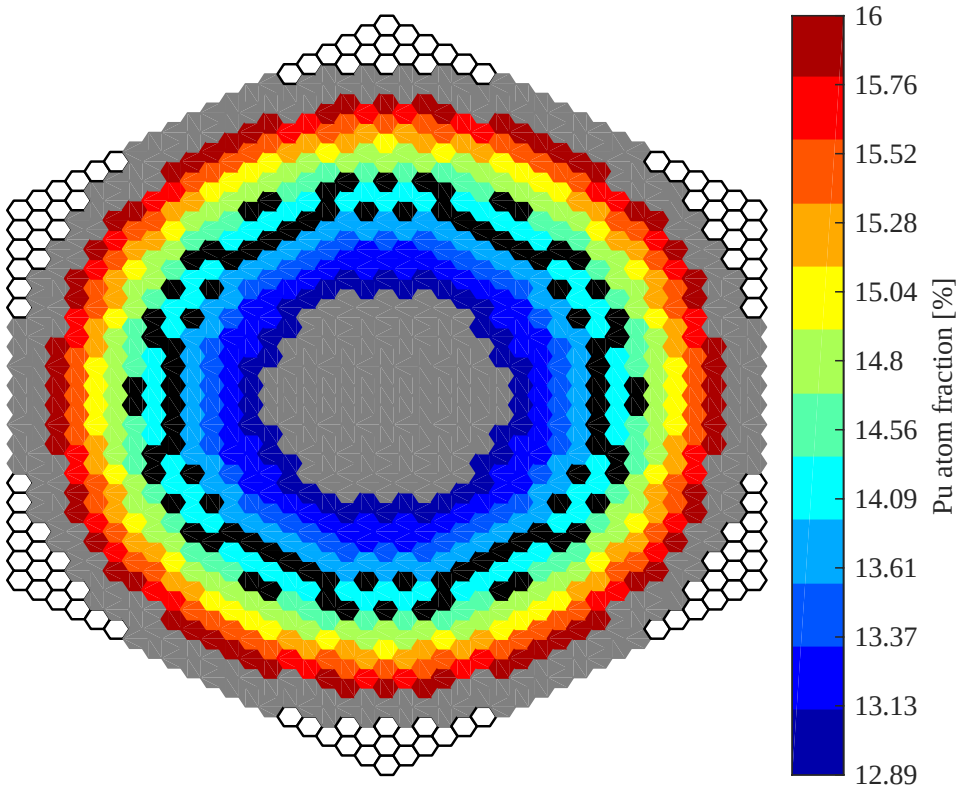

Figure S17. Core geometry and plutonium grading at axial locations z = 140–160 cm and 240–260 cm. Reflector assemblies are in gray, and fuel assemblies contained a graded plutonium concentration of 12.89 to 16 atom percent of heavy metal. Diluent assemblies are shown in black. Assembly locations in white were filled with coolant.

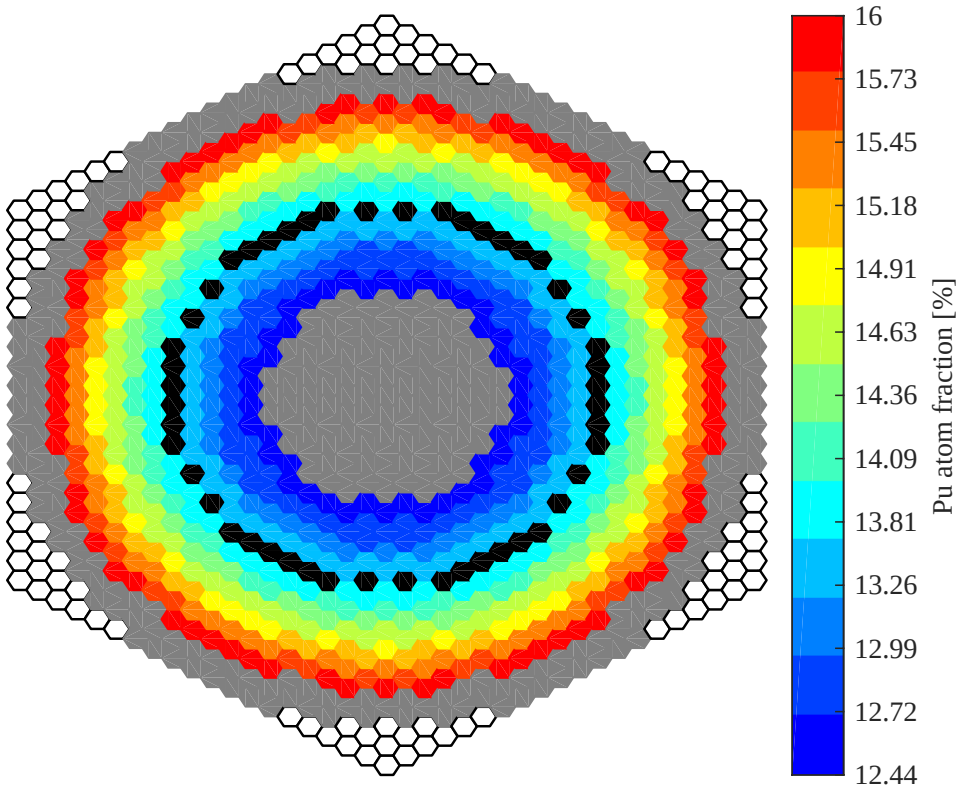

Figure S18. Core geometry and plutonium grading at axial locations z = 160–180 cm and 220–240 cm. Reflector assemblies are in gray, and fuel assemblies contained a graded plutonium concentration of 12.44 to 16 atom percent of heavy metal. Diluent assemblies are shown in black. Assembly locations in white were filled with coolant.

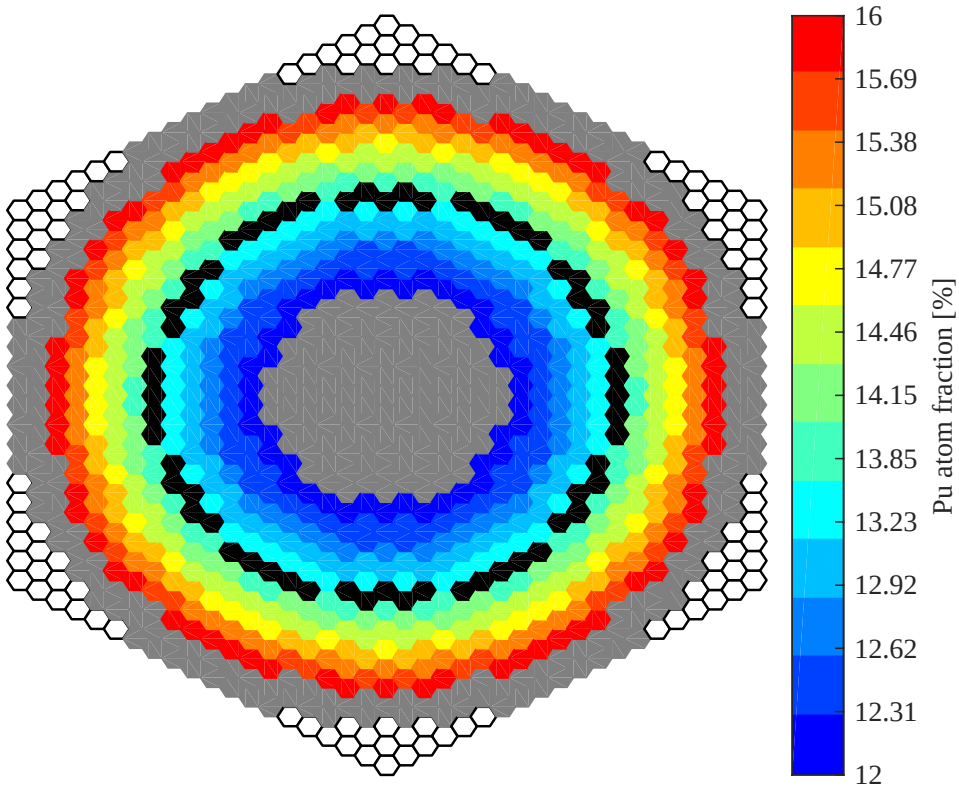

Figure S19. Core geometry and plutonium grading at axial location z = 180–220 cm. Reflector assemblies are in gray, and fuel assemblies contained a graded plutonium concentration of 12 to 16 atom percent of heavy metal. Diluent assemblies are shown in black. Assembly locations in white were filled with coolant.

Supplementary Note 4. Pin-Level Core Geometry and Materials. Figure S20 shows the geometry of the fuel and reflector pins, which is a standard design for an oxide-fueled fast reactor [2]. The fuel pins had a central void filled with helium gas, which is intended to accommodate fuel swelling due to burnup. The smear density of the pin, which is the fraction of the inner area of the cladding that contains fuel, was 75%. Figure S21 shows the arrangement of the fuel and reflector pins in each assembly. All four core designs had the same pin-level geometry in order to compare them on an even basis. The densities of the fuel pins in the unsoftened mixed oxide core, unsoftened metal core, and softened metal core were adjusted so that the overall mass of actinides in each design remained the same.

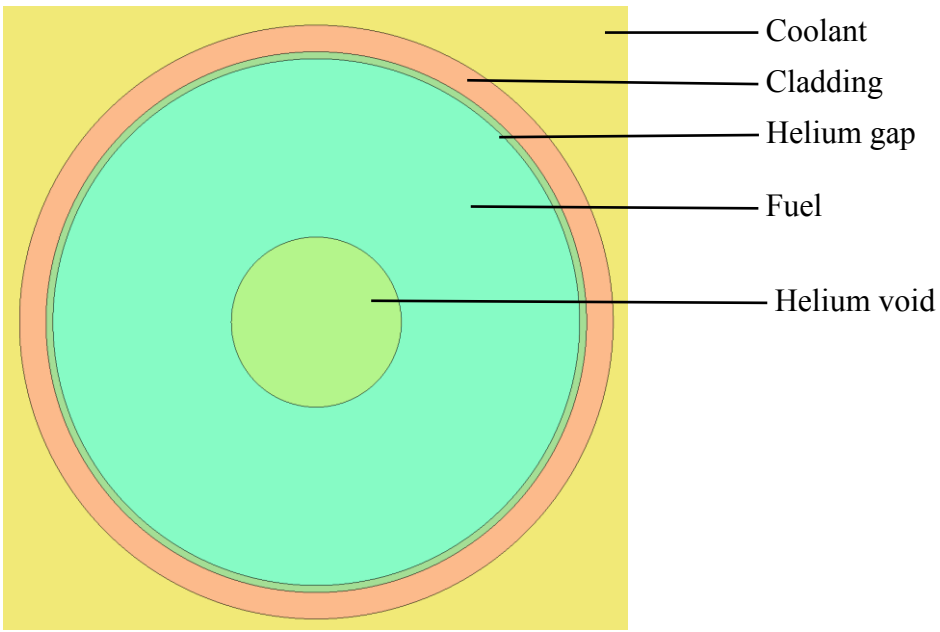

Figure S20. Fuel and reflector pin geometry. The fuel pins were annular, with inner and outer diameters of 0.24 cm and 0.75 cm, respectively. The helium gap between the fuel and the cladding was 0.01 cm wide, and the cladding was 0.038 cm thick.

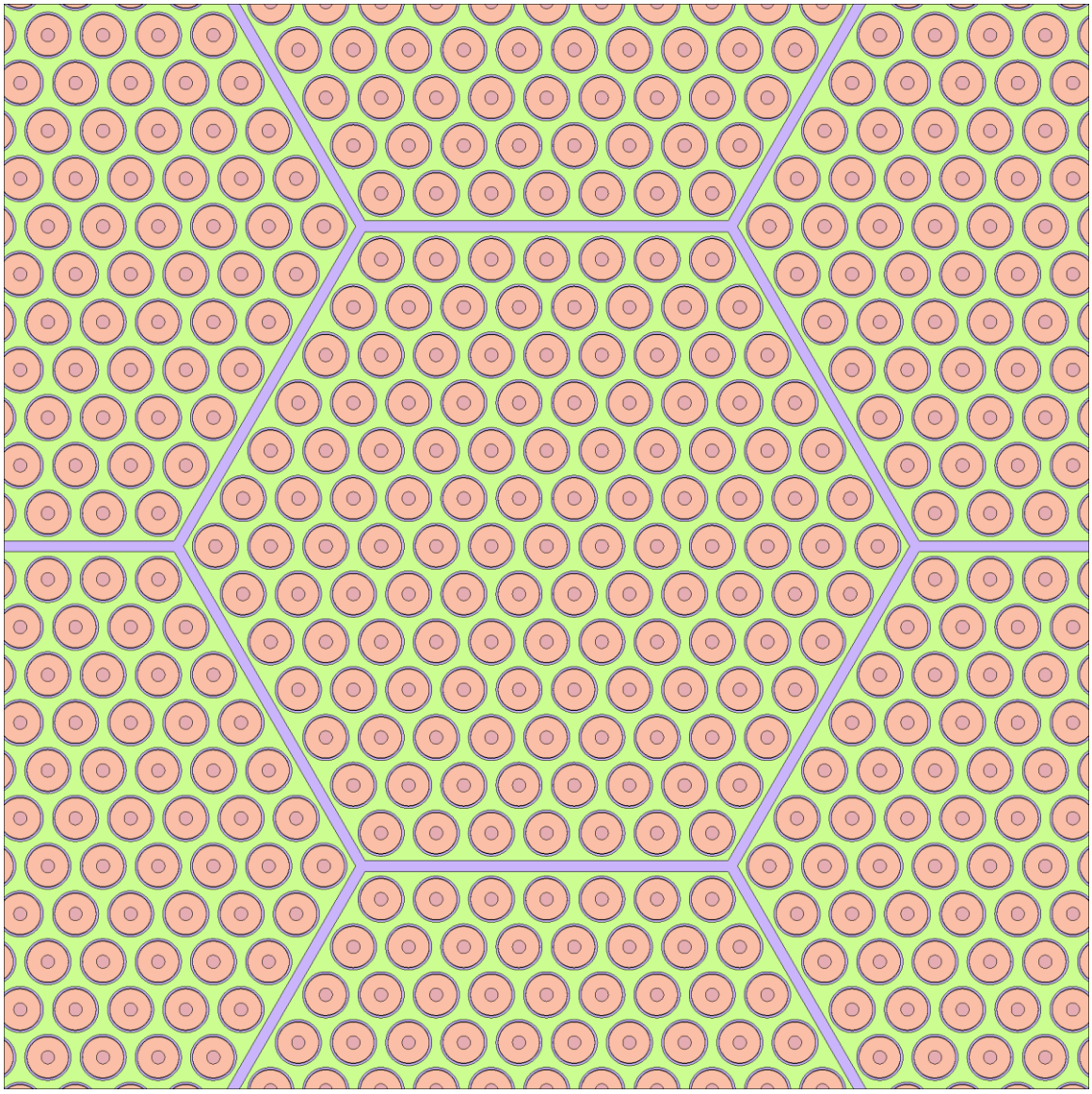

Figure S21. Assembly geometry. The fuel and reflector assemblies had the same geometry. Each hexagonal assembly contained 127 fuel or reflector pins.

Supplementary Note 5. MCNPX Cross-checks. In order to validate our results computed in Serpent 2.1.28, additional Monte Carlo calculations of the breed-burn reactor were done in MCNPX 2.7.0 [1]. The input deck used in the Serpent simulation was reproduced for execution in MCNPX, which was burned for 15 time steps of 365 days each. The flux calculations in Serpent were done using 12,000 neutrons per k_{eff} cycle, with 800 inactive and 800 active cycles. In order to fully take advantage of message passing interface (MPI) parallelization, the MCNPX simulations were done using 192,000 neutrons per k_{eff} cycle, with 50 inactive and 100 active cycles. The codes used a predictor and corrector step. In total, both simulations were done with 19.2 million neutron histories per flux calculation, or 38.4 million histories per burnup step.

In both Serpent and MCNPX, the reactor was modeled using a mesh with 10 axial and 20 radial regions, and a reflective boundary condition was applied at the axial symmetry plane. The flux from both simulations was tallied in the same 10 axial and 20 radial regions. The

fluences were computed over 8.4 simulated years, and showed good agreement (Figures S22 and S23).

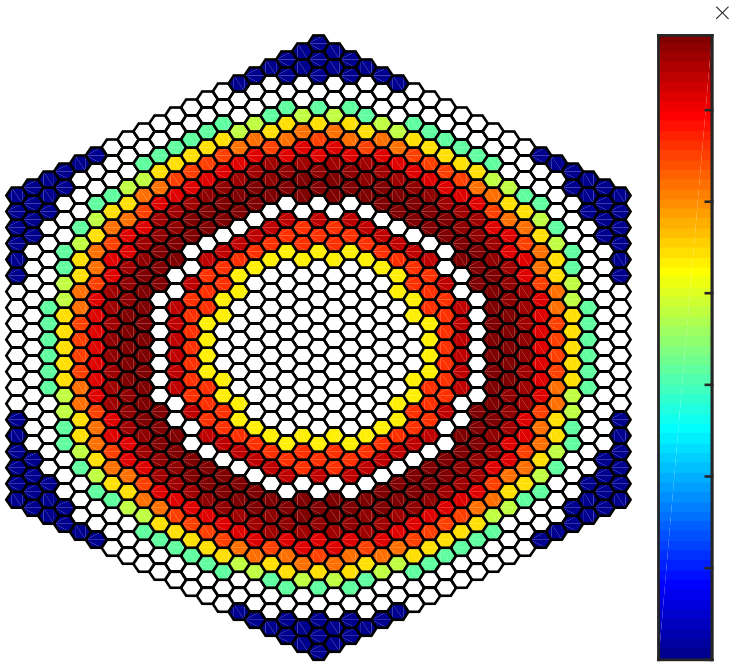

Figure S22. Neutron fluence using Serpent 2.1.28. Peak fluence was 66.2 x 10^{22} n/cm^2.

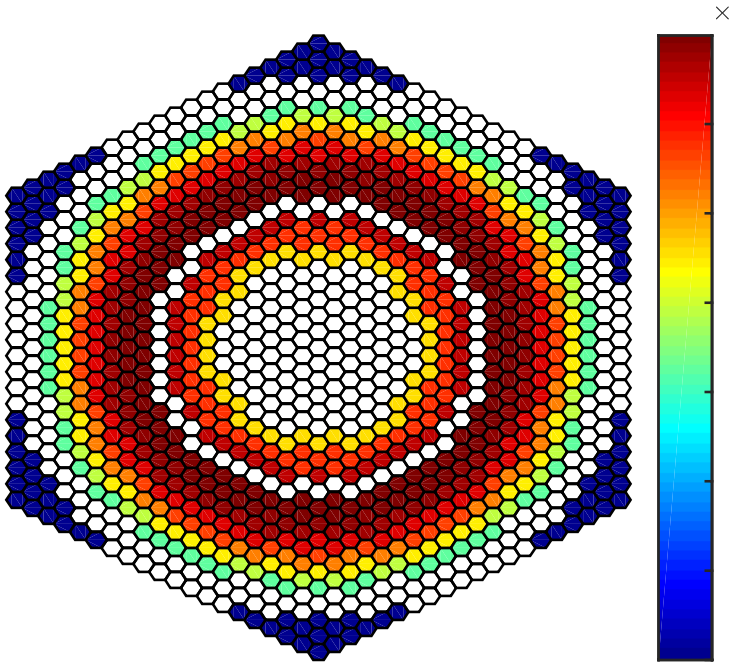

Figure S23. Neutron fluence using MCNPX 2.7.0. Peak fluence was 67.2 x 10^{22} n/cm^2.

The cumulative dpa at 8.4 years in each burnup region was also computed (Figures S24 and S25). Damage in MCNPX was computed by directly tallying the one-group dpa cross section. In Serpent, the flux was tallied in 494 groups, and combined with ENDF-B/VII.1 nuclear data

for ^{56}Fe processed with the NJOY software into 494 groups. The two codes showed good agreement, with peak dpa values in Serpent and MCNPX of 203 and 200, respectively, which was a difference of 1.5%.

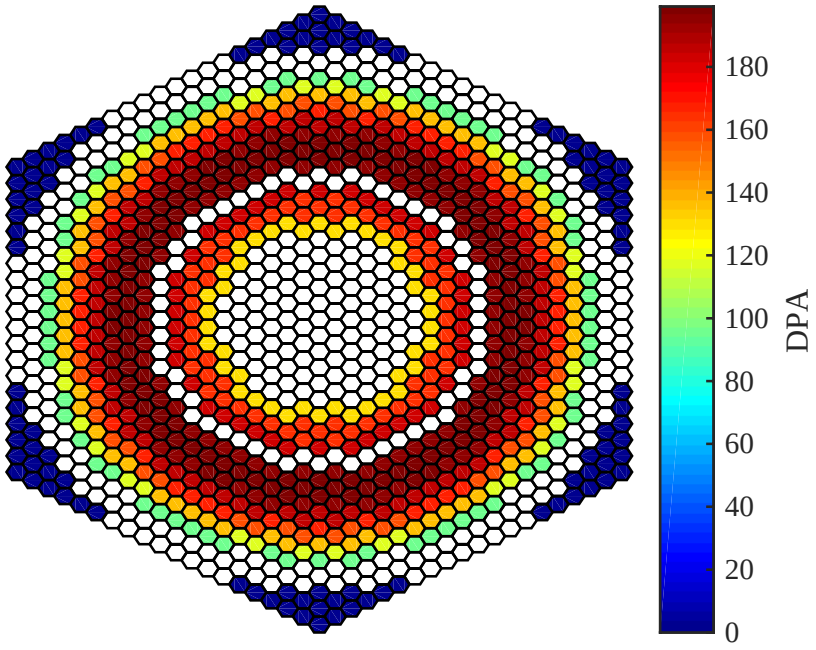

Figure S24. Cumulative dpa using Serpent 2.1.28. The peak dpa value was 203.

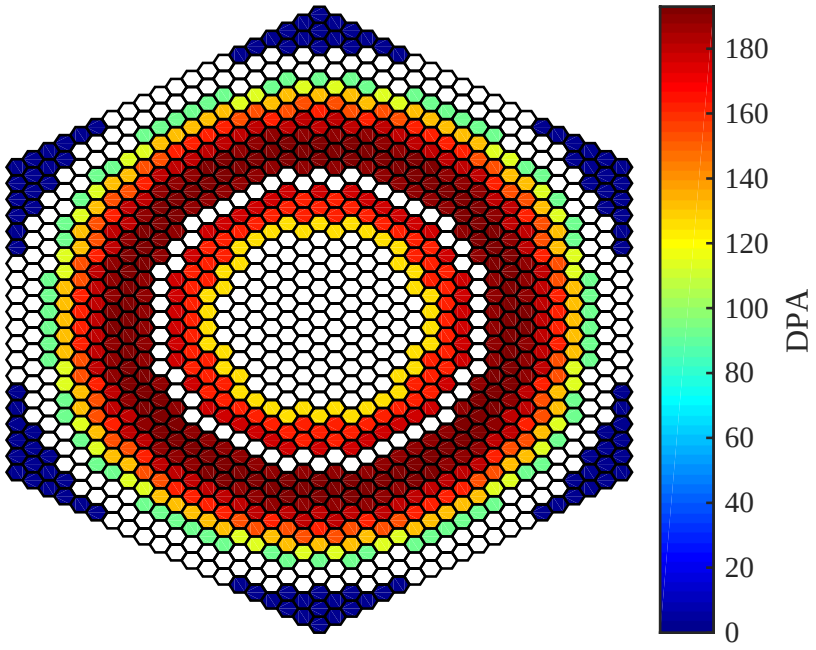

Figure S25. Cumulative dpa using MCNPX 2.7.0. The peak dpa was 200.

Supplementary Note 6. Heat transfer model. Volumetric expansion in the coolant, and the Doppler broadening of neutron cross sections are known to be the dominant mechanisms affecting fast-reactor neutronics as a result of changes in temperature [2]. The temperatures of the fuel and coolant at every axial and radial location were computed using a simple thermal resistor model [2-4]:

$$q' = \frac{\Delta T}{R}, \tag{S1}$$

where q' is the linear power density of the fuel (W/m), and R and ΔT are the thermal resistance (m-K/W) and the temperature difference (K), respectively, between the fuel and the coolant. The temperatures in the components of the unit cell between the fuel and coolant, such as the cladding and helium gap, were computed by writing Equation (S1) in terms of the individual temperature differences and thermal resistances between adjacent components:

$$T(z)_{\text{coolant}} = T_{\text{inlet}} + \int \frac{q'(z)}{\dot{m} c_p} dz, \tag{S2}$$

$$T(z)_{\text{cladding outer}} = T(z)_{\text{coolant}} + R_{\text{cladding-coolant}} q'(z), \tag{S3}$$

$$T(z)_{\text{cladding interior}} = T(z)_{\text{cladding outer}} + R_{\text{cladding outer-interior}} q'(z), \tag{S4}$$

$$T(z)_{\text{cladding inner}} = T(z)_{\text{cladding interior}} + R_{\text{cladding interior-inner}} q'(z), \tag{S5}$$

$$T(z)_{\text{fuel outer}} = T(z)_{\text{cladding inner}} + R_{\text{gap}} q'(z), \tag{S6}$$

$$T(z)_{\text{fuel inner}} = T(z)_{\text{fuel outer}} + R_{\text{fuel}} q'(z), \tag{S7}$$

where T symbols refer to temperatures (K) on the inner radial locations of each component. The symbols $\dot{m}$ and c_p are the mass flow rate (kg/s) and heat capacity (J/kg-K) of the coolant. The subscripts on T and R indicate the location at or span over which each quantity was evaluated; for example, $R_{\text{cladding outer-interior}}$ refers to the thermal resistance between the outer surface and the interior of the cladding. The resistances were obtained by solving the heat equation at steady state:

$$R_{\text{cladding-coolant}} = \frac{1}{2\pi r h_{\text{cool}}}, \tag{S8}$$

$$R_{\text{cladding outer-interior}} = \frac{\ln\left(\frac{r_{\text{clad outer}}}{r_{\text{clad interior}}}\right)}{2\pi k_{\text{clad}}}, \tag{S9}$$

$$R_{\text{cladding interior-inner}} = \frac{\ln\left(\frac{r_{\text{clad interior}}}{r_{\text{clad inner}}}\right)}{2\pi k_{\text{clad}}}, \quad \text{(S10)}$$

$$R_{\text{gap}} = \frac{1}{2\pi r_{\text{fuel outer}} h_{\text{gap}}}, \quad \text{(S11)}$$

$$R_{\text{gap}} = \frac{1}{\pi r_{\text{fuel inner}}^2 k_{\text{fuel}}}\left[\frac{1}{4}\left(r_{\text{fuel outer}}^2 - r_{\text{fuel inner}}^2\right) + r_{\text{fuel inner}}^2 \ln\left(\frac{r_{\text{fuel inner}}}{r_{\text{fuel outer}}}\right)\right], \quad \text{(S12)}$$

where r refers to radii (m), h symbols are heat transfer coefficients (W/m^2-K), and k symbols are thermal conductivity values (W/m-K). The heat transfer coefficient for sodium was drawn from the literature [5]. The heat transfer coefficient for the helium gap was estimated according to [2]:

$$h_{\text{gap}} \sim \frac{k_{\text{He}}}{\Delta r}, \quad \text{(S13)}$$

where k_{He} and Δr are the thermal conductivity (W/m-K) of helium and the width of the gap (m), respectively. The thermal conductivity of the helium was estimated using a relationship from [6]:

$$k_{\text{He}} = 15.8 \times 10^{-4} T^{0.79}, \quad \text{(S14)}$$

where T is the temperature (K) of the helium in the gap. The thermal conductivity of helium is relatively independent of pressure [5].

The thermal conductivity of the fuel was estimated using a relationship for mixed-oxide fuel with 80% U and 20% Pu [7]:

$$k_{\text{fuel}} = \frac{1}{0.037 + 2.37\text{x}10^{-4} T} + 78.9\text{x}10^{-12} T^3, \quad \text{(S15)}$$

where T is the fuel temperature (K). It was assumed that this relationship held for oxide fuel containing beryllium, at varying levels of plutonium. Thermal conductivities of the fuel and gap, and their temperatures affect each other in turn; thus, an iterative method was used where the temperature profiles were computed using a guess for k, and the average temperatures were used as an input to Equations (S14 andS15). The procedure was repeated until average fuel and gap temperatures of 1039 K and 822 K were found. These corresponded to thermal conductivities of 3.62 W/m-K and 0.32 W/m-K for the fuel and gap, respectively.

The coolant temperatures were used to adjust sodium density, and the fuel temperatures were used as inputs to the MCNPX and Serpent Doppler broadening routines. In practice, before the fuel temperatures were used as inputs to the Monte Carlo codes, they were adjusted to the nearest multiple of 100 K. This was done because Serpent holds a separate cross-section library in memory for each temperature in the input deck. As there were 200 individual regions with different temperatures, the increased memory demand would have overwhelmed the available random-access memory (RAM) on our computers.

Supplementary Note 7. Damage Model. Figure S26 shows the data that were combined in order to compute the dpa cross sections. The neutron flux was tallied by Serpent in 494 energy groups, and combined with the energy-dependent dpa cross section of iron in the same energy group structure. The dpa cross section was computed using the NJOY [8] code.

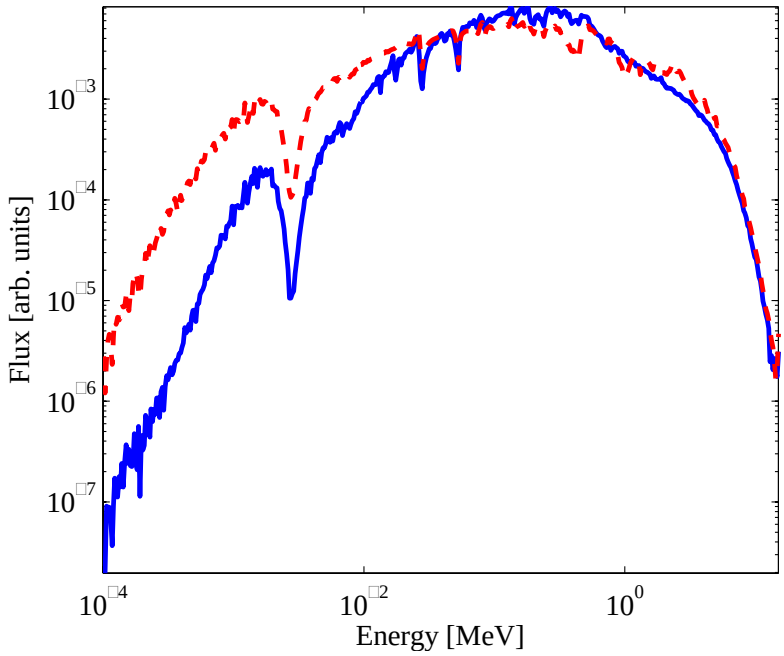

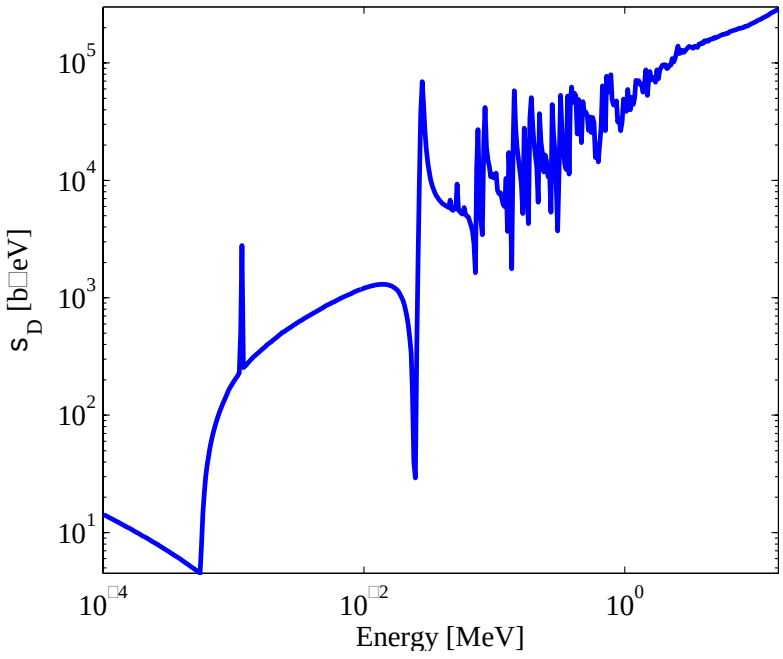

Figure S26. Damage data. Upper plot: Neutron flux spectra. The solid blue line is the neutron spectrum in a metal fueled, depleted uranium core. The dashed red line is the spectrum in a beryllium-plutonium-uranium oxide-fueled core. In both cases, the flux was tallied in 494 energy groups, and averaged over the core volume. Lower plot: Damage cross section of ^{56}Fe. The cross section was computed in 494 groups using the NJOY code, using ENDF-B/VII.1 nuclear data libraries.

Supplementary Note 8. Uncertainty calculations. The uncertainties quoted for the dpa, flux, criticality, and burnup results were computed by repeating the Monte Carlo simulation five times, each with a different random number seed, and calculating the mean and standard deviation of the results. A standard formula was used:

$$s = \sqrt{\frac{1}{N}\sum_{i=1}^{N}\left(X_i - \langle X\rangle\right)^2}\ , \qquad \text{(S16)}$$

where σ is the standard deviation, X represents one of the relevant quantities, and $N = 5$. The symbol <X> represents the geometric mean of the measured values.

The uncertainties in the reactivity coefficients were computed by applying the standard error formula on the standard deviations for k quoted using the Monte Carlo code:

$$s_\alpha = \sqrt{s_{k_1}^2\left(\frac{\partial\alpha}{\partial k_1}\right)^2 + s_{k_0}^2\left(\frac{\partial\alpha}{\partial k_0}\right)^2}\ , \qquad \text{(S17)}$$

where k_0 and k_1 are the unperturbed and perturbed values of criticality, and δ_{k1}, δ_{k0} are their standard deviations. Since Equations (4–6) have a common form, we can write:

$$\alpha = \frac{1}{k_1^2}\frac{k_1 - k_0}{\Delta P}\ , \qquad \text{(S18)}$$

where ΔP represents ΔT_{fuel}, $\Delta T_{coolant}$, or $\Delta x_{coolant}$. The partial derivatives in Equation (S17) are then given by:

$$\frac{\partial\alpha}{\partial k_1} = \frac{2k_0}{\Delta P}\frac{1}{k_1^3} - \frac{1}{\Delta P}\frac{1}{k_1^2}$$
$$\frac{\partial\alpha}{\partial k_0} = -\frac{1}{\Delta P}\frac{1}{k_1^2}\ . \qquad \text{(S19)}$$

References

1. Pelowitz, D., *MCNPX user's manual version 2.7.0*, 2011, Los Alamos National Laboratory: Los Alamos, New Mexico.
2. Waltar, A.E., D.R. Todd, and P.V. Tsvetkov, *Fast Spectrum Reactors*2012: Springer.
3. Incropera, F.P., et al., *Fundamentals of Heat and Mass Transfer, Sixth Edition* 2007, Hoboken, NJ: John Wiley & Sons.
4. Recktenwald, G.R. and M.R. Deinert, *Effect of Burnable Absorbers on Inert Matrix Fuel Performance and Transuranic Burnup in a Low Power Density Light-Water Reactor.* Energies, 2013. **6**: p. 2291-2304.
5. Lamarsh, J.R. and A.J. Baratta, *Introduction to nuclear engineering*. 3rd ed. Addison-Wesley series in nuclear science and engineering2001, Upper Saddle River, N.J.: Prentice Hall. xv, 783 p.
6. Karahan, A., *Modeling of Thermo-Mechanical and Irradiation Behavior of Metallic and Oxide Fuels for Sodium Fast Reactors*, 2009, Massachussetts Institute of Technology.
7. IAEA, *Status and Trends of Nuclear Fuels Technology for Sodium Cooled Fast Reactors*, 2011, International Atomic Energy Agency.
8. MacFarlane, R.E. and D.W. Muir, *The NJOY Nuclear Data Processing System Version 91*, 1994, Los Alamos National Laboratory: Los Alamos, New Mexico.